Determining the bulk rheological behavior of gravity-driven flow down a flume. Application to granular flows

Christophe Ancey [a] Sébastien Wiederseiner [a] Steve Cochard [b]
Martin Rentschler [a] Nicolas Andreini [a]

[a] *School of Architecture, Civil and Environmental Engineering, École Polytechnique Fédérale de Lausanne, 1015 Lausanne, Switzerland*

[b] *Department of Mathematics, University of British Columbia, Vancouver V6K 2A5, Canada*

Abstract

Determining the constitutive behavior of complex fluids (e.g., granular materials, pasty fluids) remains a delicate task. We present a general method that makes it possible to derive the bulk constitutive relation $\tau_b = F(\bar{u}, h)$ from flume experiments, where τ_b, $\bar{u}$, and h denote the bottom shear stress, mean velocity, and flow depth, respectively. Indeed, whenever a steady uniform regime is achieved, it is possible to relate the bottom shear stress, the flow depth, and the velocity. Then, after simple algebraic manipulations, we obtained a simple and systematic method to glean information on the rheological behavior. We applied this method to laboratory data obtained with dry granular flows and showed that different constitutive relations can be used to describe the same data. We found that a generalized Coulomb relation in the form $\tau_b = \mu\sigma_b$, with σ_b the bottom normal stress and $\mu \propto (\bar{u}/h^{3/2})^{1/5}$ the bulk friction coefficient, offers a convenient representation of the rheological behavior for a wide range of flow conditions and is supported by theoretical arguments. However, this relation cannot explain the constancy of the front velocity observed experimentally. Another relation in the form $\tau_b = \mu\sigma_b$ with $\mu \propto \bar{u}^{1/5}$ performs better for steep slopes or when there is a flow-depth gradient, is in good agreement with the data available to date, but is more difficult to understand from a rheophysical point of view.

Key words: constitutive equation, shallow-flow equations, rheometry, granular flow

1 Introduction

A number of natural flows involving the mass movement of a fluid or bulk material down a sloping bed can be reasonably well described within the framework of fluid mechanics. Typical examples are provided by river floods [1], snow avalanches [2–4], debris flows [5, 6], mudflows [7, 8], lava flows [9, 10], and granular flows such as rock falls [11, 12]. Among the numerous problems about the fluid-mechanics approach, the constitutive equation of complex materials is likely to be the most problematic issue [13, 14].

Admittedly there are some circumstances where one is very satisfied with an empirical equation, which accounts for the flow or rheological properties. This is quite common for instance in hydraulics when the sole objective is to compute the discharge equation, i.e. the relation between the flow depth and rate, through a given cross-section in a river. In theory, this relation could be obtained by solving the full Navier-Stokes equation or mean-flow equations supplemented by appropriate closure equations for turbulence; in practice, engineers settle for using empirical relations such as the Darcy-Weisbach or Manning-Strickler equation, whose accuracy is considered satisfactory for practical purposes.

On some occasions, there are so many impediments to a full rheological characterization that one must use empirical relations for lack of a better expedient. For instance to experimentally determine the rheological behavior of complex materials (e.g., concrete, pastes, suspensions), several authors followed the methodology usually applied to industrial fluids using laboratory or specifically designed rheometers, but the results are difficult to reproduce and may also be difficult to interpret because of significant changes inside the bulk (e.g., chemical alteration, grain sorting, compaction). Theoretical investigations encounter similar difficulties. A typical example is provided by dry granular flows, which will serve as the prototype of complex materials here. Most sound results on granular flows have been obtained for limiting regimes: on the one hand, the quasi-static, rate-independent, *frictional* regime has received much attention, in particular from soil mechanicians, who extended the earlier ideas of Mohr and Coulomb to develop the framework of elastoplasticity [15]. On the other hand, the fully dynamic rapid dilute flow regime has been investigated using the kinetic-theory framework [16, 17], which emphasizes the role played by velocity fluctuations (granular temperature) and collisions in the stress generation. A key issue is that many granular flows of practical interest in nature or industry occur in an intermediate, transitional flow regime, often called the *frictional-collisional* regime, which lies between these two limiting regimes. A number of empirical approaches have been proposed to model dry granular flows in a frictional-collisional regime. The simplest idea was to patch together the constitutive equations from the two limiting flow

regimes. For instance, Savage [18] computed the total stresses as the sum of a frictional Coulomb contribution and a rate-dependent contribution arising from particle collisions and derived from kinetic theory in the dense-regime limit. Several authors have elaborated on this preliminary model to provide related models, which are in good qualitative and/or quantitative agreement with flume experiments [19–23]. An obvious shortcoming of these models lies in the linear combination of frictional and collisional stresses, since numerical simulations reveal a much more complex interplay between frictional and collisional interactions [e.g., see 24–26]. Various models have been proposed to take into account a nontrivial coupling between frictional and collisional interactions in a dense granular flow. For instance, Mills et al. [27] modeled dry granular flows as the motion of a network of transient solid chains through an assembly of particles behaving as a viscous or Bagnold (i.e., collisional regime) fluid. Using dimensional arguments on the characteristic times associated with friction and collision, Ancey and Evesque [28] suggested that the interplay between the frictional and collisional contributions is governed by the Coulomb number (also called the inertial number in subsequent publications). Since then, numerical simulations and experimental data have supported this idea [29]. More recently, Jop et al. [30] synthesized earlier results into a generalized Bingham constitutive equation.

In this paper, we will show how we can obtain such empirical relations describing the bulk rheological properties of complex materials in a systematic and consistent way, at least for modeling gravity-driven flows. The strategy pursued here is to use depth-averaged governing equations [see Eqs. (3–5)] and a relation $\tau_b = F(\bar{u}, h)$ as a bulk substitute of the constitutive equation $\tau = f(\dot{\gamma},\ \sigma)$ for simple shear flows, where τ, τ_b, $\bar{u}$, h, $\dot{\gamma}$, and σ denote the shear stress, the bottom shear stress, the flow-depth averaged velocity, the flow depth, the shear rate, and the normal stress, respectively. When the flow reaches a steady regime, where gravity acceleration is balanced by the frictional force, the equation relating the mean velocity and flow depth depends solely on bed slope θ. Since in the meantime, the bottom shear stress for a steady uniform regime is $\tau_b = \rho g h \sin\theta$, eliminating slope from both equations leads to the desired relation $\tau_b = F(\bar{u}, h)$. We first explain how to derive the relation $\tau_b = F(\bar{u}, h)$ from $\bar{u}$ and h measurements. The method is assumed to be valid for a fairly wide range of flow conditions, for which the shallow-flow equations provide a reasonable description. Since very few field data providing $\bar{u}$ and h are available to date, we will apply our method to laboratory data. In § 3, we shall use the data obtained by Pouliquen [31], Ancey et al. [32], and Ancey [33] with dry granular flows (glass beads) on rough surfaces. This example can be highly valuable in understanding subtle points in the rheological interpretation of data. We will see that very different constitutive equations can be proposed on the sole basis of these experimental data. Additional properties of the flows investigated must be used to differentiate the candidates. In § 4, we will focus our attention on the front velocity together with the flow-depth

profile within the head. We will see that none of the constitutive equations proposed to date for modeling granular flows is consistent with experimental observations. We will also show that a Coulomb-like equation with a velocity-dependent friction coefficient is more successful, but is questionable when one tries to interpret it physically.

2 Governing equations and method

2.1 Deriving the bulk constitutive equation

We investigate two-dimensional gravity-driven flows down rough inclined surfaces. Figure 1 shows the typical flow-depth profile, which is an idealization of flows in a natural or laboratory setting. The surface is a planar rough plane tilted at an angle θ. The flow is infinite in the transverse direction, i.e., any sidewall effect is ignored. The bottom surface is rough enough for the velocity at the flow base to be zero.

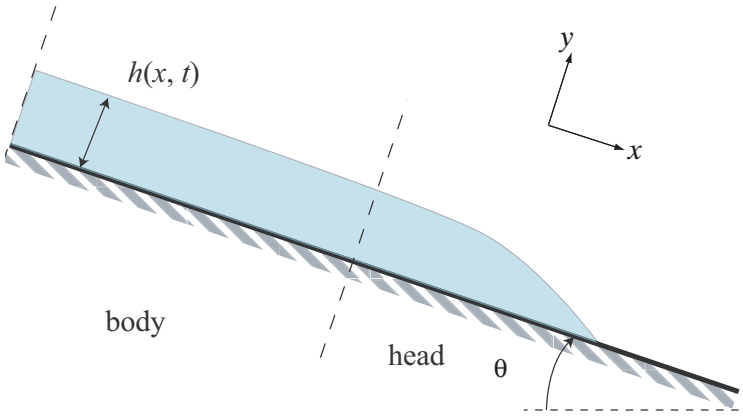

Fig. 1. Sketch of a gravity-driven flow down an inclined plane.

We start from the local (Cauchy) mass and momentum balance equations

$$\frac{\partial u}{\partial x} + \frac{\partial v}{\partial y} = 0, \tag{1}$$

$$\rho \frac{d\mathbf{u}}{dt} = \rho \mathbf{g} + \nabla \cdot \boldsymbol{\sigma}, \tag{2}$$

where d/dt denotes the material derivative, $\mathbf{u} = (u, v)$ the velocity field, and $\boldsymbol{\sigma}$ the stress tensor. Integrating Eqs. (1–2) across the flow depth leads to the flow-depth averaged mass and momentum equations (also called the Saint-Venant equations)

$$\frac{\partial h}{\partial t} + \frac{\partial h\bar{u}}{\partial x} = 0, \tag{3}$$

$$\rho\frac{\partial h\bar{u}}{\partial t} + \rho\frac{\partial h\overline{u^2}}{\partial x} = \rho g h\sin\theta - \tau_b + \frac{\partial h\bar{\sigma}_{xx}}{\partial x}, \tag{4}$$

$$-\rho g\cos\theta(h-y) = \sigma_{yy} \tag{5}$$

where $\bar{u} = h^{-1}\int_0^h u(x,\ y,\ t)dy$ and $\bar{\sigma}_{xx} = h^{-1}\int_0^h \sigma_{xx}dy$ denote the flow-depth averaged velocity and downstream normal stress, respectively; $\tau_b = \sigma_{xy}(y=0)$ is the bottom shear stress. To derive these equations, we have assumed that the ratio $\epsilon = H_*/L_*$ is small, where H_* and L_* represent typical flow-depth and flow-length scales, and the normal stresses σ_{xx} and σ_{yy} vanish at the free surface, i.e., there is neither resisting action of the ambient fluid, nor surface tension; for more details on this derivation, see the recent papers by Bouchut et al. [34] and Keller [35]. Note that Eq. (3) is exact and is the equivalent of the continuity equation on the bulk scale. Equation (4) is the momentum equation projected onto the x-axis; it is valid to the leading order $O(\epsilon)$. If the head of the flow is characterized by a significant increase in the free-surface curvature, the bulk momentum equation is, in principle, no longer valid. Equation (5) is the y-projection of the bulk momentum equation; to order $O(\epsilon)$, this equation is algebraic and states that the normal stress σ_{yy} varies linearly with flow depth.

Additional assumptions are needed to close the governing equations. The first one consists in relating the mean square velocity $\overline{u^2}$ to the flow-depth averaged velocity $\bar{u}$. This is usually done by introducing the Boussinesq coefficient $\beta = \overline{u^2}/\bar{u}^2$ and assuming it to be constant. Another assumption commonly used for geophysical and dense granular flows concerns the computation of the mean normal stress $\bar{\sigma}_{xx}$. We assume that the streamwise averaged component $\bar{\sigma}_{xx}$ is linearly related to the mean cross-stream component $\bar{\sigma}_{yy}$: $\bar{\sigma}_{xx} = k\bar{\sigma}_{yy} = -k\rho g h\cos\theta/2$, where k is a constitutive parameter, sometimes called the active/passive coefficient by reference to soil mechanics [11]. With these assumptions and using the bulk mass balance equation (3), we end up with a momentum equation in the form

$$\frac{\partial\bar{u}}{\partial t} + (2\beta-1)\bar{u}\frac{\partial\bar{u}}{\partial x} = g\sin\theta - \frac{\tau_b}{\rho h} - \left(kg\cos\theta + (\beta-1)\frac{\bar{u}^2}{h}\right)\frac{\partial h}{\partial x}. \tag{6}$$

Equation (6) can be used backwards to gain insight into the rheological behavior. When a steady regime is achieved, we can derive a bulk constitutive relation in the form $\tau_b = F(\bar{u}, h)$ if we have information on the body behavior, e.g., the relation between the flow-depth averaged velocity (or the flow rate per unit width $q = \bar{u}h$) and the flow depth. Indeed, if the body is in a steady uniform regime, Eq. (6) or (4) shows that the bottom shear stress

$$\tau_b = \rho g h\sin\theta, \tag{7}$$

is independent of the constitutive equation; similarly, the bottom normal stress σ_b satisfies: $\sigma_b = \rho g h \cos\theta$, whatever the material. Let us imagine now that there is a one-to-one relation between the shear rate $\dot{\gamma} = du/dy$ and the shear stress $\tau = \rho g(h-y)\sin\theta$: $\dot{\gamma} = f(\tau)$. Integrating this equation twice across the flow depth provides the flow-depth averaged velocity $\bar{u} = h^{-1}\int_0^h dy \int_0^y f(\eta)d\eta$. We end up with an expression that can usually be cast in the form of a combination of power monomials

$$\bar{u} = Ah^n(g\sin\theta)^m, \tag{8}$$

with A, n, and m three constitutive parameters. This equation may be exact (e.g., for Newtonian and power-law fluids) or an approximation of a more complex form (see § 2.3). In order to obtain a bulk constitutive relation between τ_b and the flow variables ($\bar{u}$, h), we eliminate $\sin\theta$ from Eqs. (7) and (8) and find

$$\tau_b = \rho h \left(\frac{\bar{u}}{Ah^n}\right)^{1/m}. \tag{9}$$

Without providing the true constitutive relation, this relation can be used to (i) yield a bulk constitutive equation that reflects the mean features of the flow curve $\dot{\gamma} = f(\tau)$ for simple-shear experiments, as shown in § 2.3, and (ii) provide the bottom shear expression needed in the shallow-flow equations (3) and (6).

In § 4, we will see another application of the shallow-flow equations. Essentially, the idea is that the front velocity and the flow-depth profile of the head can be used as additional elements to obtain information or test rheological interpretations.

2.2 Comments

The derivation of the bulk constitutive equation (9) deserves a few comments.

First, we are able to obtain a rough idea of the structure of the constitutive equation by eliminating the slope θ from Eqs. (7–8). Basically, Eq. (7) is a consequence of the momentum balance for a steady uniform flow; this equation is independent of the rheological behavior. In contrast, Eq. (8) reflects both the shear stress distribution (imposed by the momentum balance equation) and the constitutive equation. Since the constitutive equation must be frame-independent (i.e., it must hold for any coordinate system), channel inclination

cannot be used as a constitutive variable and we then eliminate it from Eqs. (7–8) to obtain what we call the bulk constitutive equation.

Second, the treatment here follows the classic approach taken in rheometry to recover the constitutive equation of simple fluids from bulk measurements. As a consequence, it inherits some of its strengths and weaknesses. In rheometry, *simple fluids* are introduced as an idealized class of incompressible fluids, for which the stress tensor $\mathbf{s}$ is determined, to within a pressure term, by the history of the strain-rate tensor $\mathbf{d}$: $\mathbf{s} = \mathcal{F}(\mathbf{d})$, where $\mathcal{F}$ is a function [36]. Typical examples include incompressible Newtonian fluids, Bingham (viscoplastic) materials, or Oldroyd (viscoelastic) fluids. A counter-example is a suspension of coarse particles in a Newtonian fluid since additional variables (e.g., solid concentration) are needed to fully characterize the stress state. The fundamental assumption of rheometry is that experimentally, we can create viscometric flows, where the kinematic conditions are the simple ones we can image: there is a relative deformation gradient that is linear with time at any point of the material [36]. Flows down infinite channels (i.e., when finite-size effects can be ignored) are a typical example of viscometric flow. The important point is that for simple fluids in a viscometric flow, one can relate bulk quantities (i.e., flow rate and flow depth) to local quantities (shear rate, shear stress), which means that the constitutive equation can be inferred from measurements. To date, only viscometry theory can achieve this in a systematic and rigorous way. The major shortcoming is that many complex fluids do not enter the class of simple fluids. In the next section, we will see how critical this assumption of simple fluids is when dealing with complex materials. For these materials, there is no easy way of retrieving the constitutive equation from bulk measurements. An increasingly popular approach to get around this obstacle is to use visualization techniques in viscometric flows to directly obtain the constitutive equation by measuring the velocity profile, which is rarely possible for natural flows or complex materials.

Third, the scaling relation (8) is not a result that can be derived mathematically, but rather is an approximation, which usually performs well. Indeed, fundamental physical laws are expressible in terms of power monomial functions because all functional relations between physical variables must be invariant under a stretching of the dimensions of these variables [37]. As shown through an example in the next subsection, this scaling relation can mimic the behavior of nontrivial constitutive equations. A typical example in a related context is provided by the Manning-Strickler relation used in open-channel hydraulics to compute the bottom shear stress for turbulent water flows down a rough boundary; in that case, τ_b is expressed as $\tau_b = \rho g \bar{u}^2/(K^2 h^{1/3})$, with K the Strickler coefficient, which depends on bed roughness. Physically, the bottom shear stress depends on the structure of the velocity profile close to the boundary (logarithmic boundary layer), while the flow-depth averaged velocity depends on the turbulence structures on a larger scale and thus cannot be com-

puted exactly. However, it has long been recognized that for open channels, the vertical profile of flow velocity can still be closely approximated by a logarithmic profile, even far from the bottom. This led Keulegan [38] to consider the mean velocity a logarithmic function of the flow depth: $\bar{u} = u_* \ln(11h/k_s)/\kappa$ with $u_* = \sqrt{\tau_b/\rho}$ the shear velocity, k_s the roughness size, and κ the von Kármán constant. Inverting this relation gives the bottom shear stress as a function of $\bar{u}$ and h: $\tau_b = \rho\kappa\bar{u}^2/\ln^2(11h/k_s)$. The Manning-Strickler relation is retrieved by noting that for shallow flows, $\ln h$ behaves like $h^{1/6}$. Note that historically, the Manning-Strickler relation was worked out by trial and error by correlating flow resistance data with $\bar{u}$ and h. This example shows that a power monomial function can be used to describe the bottom shear stress of complex flows.

2.3 Numerical application

We first address the simple case of a Newtonian fluid of viscosity μ. Integrating the relations $\tau = \rho g(h-y)\sin\theta = \mu\dot{\gamma}$ gives $\bar{u} = Ah^n(g\sin\theta)^m$ with $A = \rho g/(3\mu)$, $n = 2$, and $m = 1$. Eliminating θ from this equation and Eq. (7) gives $\tau = 3\mu\bar{u}/h$, which mimics the true flow curve $\tau = \mu\dot{\gamma}$ by posing $\dot{\gamma} \approx \bar{u}/h$; in fact, since the velocity profile in the cross-stream direction is not constant, the approximation $\dot{\gamma} \approx \bar{u}/h$ provides the bottom shear rate to within a multiplicative constant (3 for a Newtonian fluid), which depends on the fluid at hand.

We now consider the more complex case of a Herschel-Bulkley fluid, whose constitutive relation reads $\tau = \tau_c + \kappa\dot{\gamma}^p$ for $\tau > \tau_c$ and $\dot{\gamma} = 0$ for $\tau \leq \tau_c$, with τ_c the yield stress, κ a consistency parameter, and p the shear-thinning exponent. Again, integrating these relations twice provides the flow-depth averaged velocity

$$\bar{u} = \frac{p}{p+1}\sqrt[p]{\frac{\rho g\sin\theta}{\kappa}}h_c^{1/p+1}\left(1 - \frac{h_c}{h}\frac{p}{2p+1}\right), \tag{10}$$

with $h_c = h - \tau_c/\rho g\sin\theta$. Since this relation is nonlinear, we cannot transform it into a combination of monomials, but in practice for a particular set of values p, κ, and τ_c, an approximation in terms of monomials can easily be found numerically, which fits the data reasonably well (i.e., with a relative deviation of a few percent). Taking $\tau_c = 50$ Pa, $\kappa = 20$ m s$^{1/3}$, and $p = 1/3$ (typical values for a mud suspension), we generated 20 data corresponding to 5 deg, 10 deg, 15 deg, and 20 deg slopes and flow depth within the range 2–10 cm. We then fitted Eq. (8) on these data and found: $m = 5.57$, $n = 6.62$, and $A = 8.08 \times 10^6$ m$^{-11.2}$ s$^{10.1}$. This led to a bulk shear stress in the form

$$\tau_b = 87 \left(\frac{\bar{u}}{h}\right)^{0.19} \approx 87\dot{\gamma}^{0.19}. \tag{11}$$

Figure 2 reports the theoretical flow curve together with its bulk estimate (11). Equation (11) captures the salient characteristics of the flow curve, although it does not involve any yield stress. As for the Newtonian case, there is a departure between both curves since in Eq. (11), the shear rate is approximated by $\dot{\gamma} \approx \bar{u}/h$, i.e., we replace the actual shear rate with a flow-depth averaged value. Note that in numerical applications with ideal cases, only a few data (with a minimum of 10–20 values) are required to obtain a reliable approximation of the mean velocity, then the bulk shear stress.

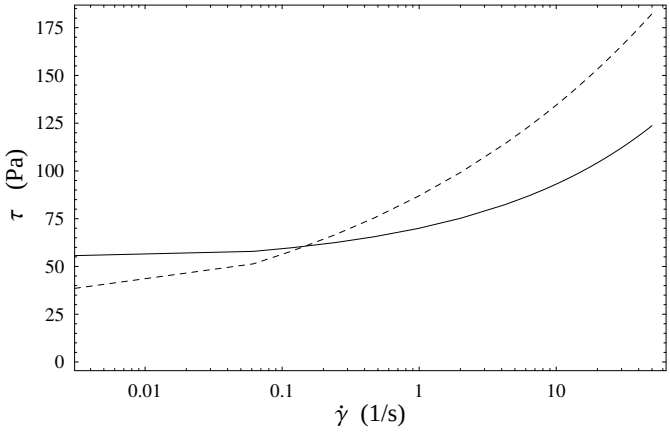

Fig. 2. Comparison between the theoretical flow curve (solid line) $\tau = \tau_c + \kappa\dot{\gamma}^p$ ($\tau_c = 50$ Pa, $\kappa = 20$ m s$^{1/3}$, and $p = 1/3$) and the its bulk estimate (dashed line) given by Eq. (11).

3 Application to laboratory experiments

3.1 Data source

We applied our method to three sets of data stemming from experimental investigations conducted by Pouliquen [31], Ancey et al. [32], and Ancey [33]. Pouliquen [31] studied dense granular avalanches down a 0.7-m-wide, 2-m-long plane. The inclination range was 22–28 deg. The flow rate per unit width ($q = h\bar{u}$) ranged from 0.1 to 3.2 l m^{-1} s^{-1}. The bulk was made up of monosized glass beads. Initially, all the material was contained in a box closed by a sluice gate and placed at the plane inlet. At time $t = 0$, the door was lifted up and the material was unleashed down a rough incline. Keeping the same aperture made it possible to obtain a steady inflow. The flow was made up of two parts: a body and a head (see Fig. 1). Within the body, since the flow depth was

uniform, a steady uniform flow regime was achieved. Using a laser sheet and high-speed video camera, Pouliquen [31] measured the flow-depth profile and the velocity of the front. He observed that the front moved downwards at constant velocity; the contact line at the front was a straight line. The front velocity scaled as $u_f \propto h^{3/2}$. He also found that his experimental data fell onto a master curve when he scaled the mean velocity $\bar{u}$ ($\bar{u} = u_f$) by $\sqrt{gh}$ and the flow depth by $h_{stop}(\theta)$, where h_{stop} denotes the thickness of the grain layer deposited along the bed when the flow stopped

$$\frac{\bar{u}}{\sqrt{gh}} = \kappa \frac{h}{h_{stop}(\theta)}, \tag{12}$$

where κ is a constant and h_{stop} is expressed as a function of the bed slope θ:

$$h_{stop}(\theta) = Ld \ln \left(\frac{\tan\theta_2 - \tan\theta_1}{\tan\theta_2 - \tan\theta} \right), \tag{13}$$

with d the particle diameter, L a dimensionless parameter, $\tan\theta_2$ the bed slope for which no deposition occurs and $\tan\theta_1$ the minimum bed slope for a steady uniform flow to occur. Making use of the relation $\mu = \tan\theta$ holding for all steady uniform flows, where $\mu = \tau_b/\sigma_b$ is the bulk friction coefficient (it does depend on both bed and material properties), he proposed an expression for μ in the form

$$\mu(\bar{u}, h) = \tan\theta_1 + (\tan\theta_2 - \tan\theta_1) \exp\left(-\frac{\kappa}{L} \frac{h}{d} \frac{\sqrt{gh}}{\bar{u}} \right). \tag{14}$$

The bottom shear stress is then: $\tau_b = \mu(\bar{u}, h)\sigma_b$. Here we will use the data corresponding to material 1 (glass beads 0.5 mm in diameter) in Pouliquen's paper since the raw data were provided. For this material, he found the following estimates of the constitutive parameters: $L = 1.96$, $\theta_1 = 20.7$ deg, $\theta_2 = 32.8$ deg, and $\kappa = 0.136$.

Other sets of data were obtained by Ancey et al. [32] with a narrow channel (width $W = 25$ mm) and Ancey [33] with a wider channel (width $W = 48$ mm). Each flume was 2 m long. The flow was supplied in material from a hopper with a constant inflow rate. The flow rate was controlled by the hopper gate and ranged from 0.3 to 28 l m^{-1} s^{-1}. The flow depth was measured with ultrasonic sensors. The channel inclination varied from 24 to 37 deg. Ancey used glass beads and sand, with a diameter ranging from 0.3 to 2 mm. The most striking feature was the great variability of the discharge curves with respect to the particle diameter, the roughness size, and the channel slope. Any attempt to classify fully developed flows is rendered difficult by this sensitivity of the experimental data to even small changes in the control parameters (slope, roughness). A crude classification of the discharge curves could be the following. For an inclined channel, whose roughness is made up

of particles with the same diameter as the flowing particles, there are two regimes. The first regime, called regime A, occurred at low discharges and was characterized by a discharge equation in the form $q \propto h^n$, with n usually close to 2.5 (but it could also be in the range $2-3$); the velocity profile was fairly linear. The second regime, referred to as regime B, occurred at high discharges and it was characterized by a fairly linear discharge curve since the flow depth varied as $q \propto h^n$, with n ranging from 0.97 to 1.16; the velocity profile was clearly convex. The transition from regime A to regime B was described using a critical Froude number $Fr = \bar{u}/\sqrt{gh}$. The critical Froude number was a function of both slope and bed roughness. The critical Froude number was reached, but not exceeded. Indeed, when flow was generated with a small flow depth (namely in regime A), the Froude number rose as $Fr \propto h^p$, with p close to 1, as the flow depth increased. When the critical Froude number was reached, there was a transition from regime A to regime B. For regime B, the Froude number decreased as $Fr \propto 1/\sqrt{h}$ as the flow depth increased. For 1-mm and 0.36-mm glass beads, the critical Froude number curves were very close [see Fig. 16, 33]; in terms of flow rate, the transition from regimes A to B occurred for q in the range 4 to 10 l m^{-1} s^{-1} depending on slope and bed roughness. Note that according to this partitioning, the flows observed by Pouliquen were in regime A.

3.2 Simple-fluid approximation

Using Pouliquen's experimental measurements, we found that the mean velocity scaled as

$$\bar{u} = 0.072 h^{1.42} (g \sin\theta)^{5.78}.$$

For the sake of simplicity, we posed $n = 3/2$ and $m = 6$ in Eq. (8) (giving $A = 0.077$ s^{11} m$^{-13/2}$). We then obtained

$$\tau_b \propto \bar{u}^{1/6} h^{3/4}. \tag{15}$$

In Fig. 3, we plotted the variation in $J = u^{1/6}h^{3/4}$ with τ_b. Over the entire experimental range, Fig. 3 shows a remarkable linearity between $J = u^{1/6}h^{3/4}$ and τ_b. Note that when the data scaled with J, the scattering around the mean trend is much lower than the scattering exhibited when using the scaling originally proposed by Pouliquen [31].

We also checked this scaling with Ancey's data. Figure 4(a) shows the J variation with τ_b for 0.35-mm glass beads flowing down a 25-mm-wide channel

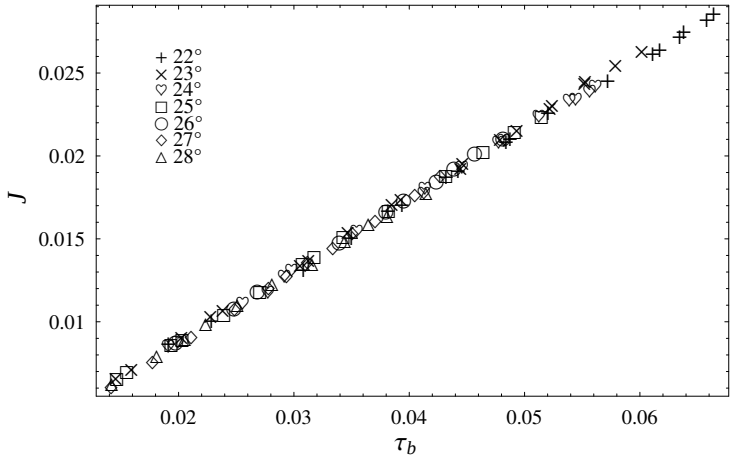

Fig. 3. Variation in $J = u^{1/6}h^{3/4}$ with $\tau_b = \rho g h \sin\theta$ for Pouliquen's data [31] (material 1).

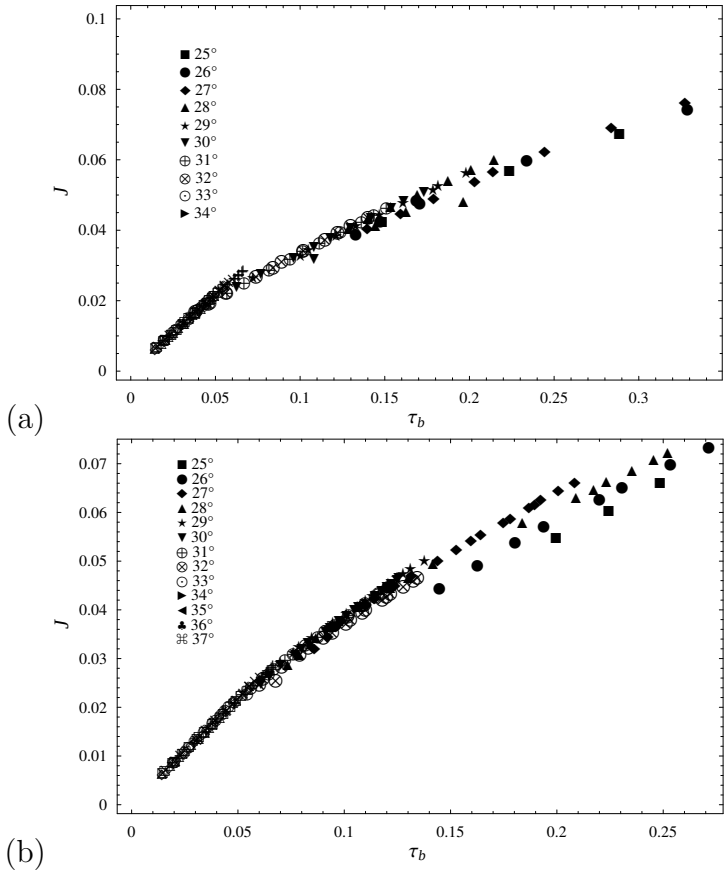

Fig. 4. Variation in $J = u^{1/6}h^{3/4}$ with $\tau_b = \rho g h \sin\theta$ (a) 0.35-mm glass beads [32], 1-mm glass beads [33]. Pouliquen's data are also reported for completeness (same caption as in Fig. 3).

[32], whereas Fig. 4(b) shows the data obtained with 1-mm glass beads flowing down a 48-mm-wide channel [33]. In both cases, the behavior is roughly linear, but some departure from the linear trend is seen for shallow slopes (slopes from 25 deg to 27 deg). Quite remarkably, the data sets match reasonably well with Pouliquen's data, although they were obtained using very different experimental regimes (both regimes A and B are reported in Fig. 4). The match is particularly good with 1-mm glass beads.

3.3 Alternative representation

An interesting question concerns the interpretation of the scaling (15). Usually, one is satisfied when the $\bar{u}/h$ ratio arises, since it can be interpreted as a bulk estimate of the shear rate. This is not the case here and, moreover, the structure of relation (15) differs substantially from that usually measured for classic fluids. Since the material is granular, we can imagine that the shear stress exhibits a dependence on both the shear rate and normal stress: $\tau = f(\dot{\gamma})\sigma$, as suggested by a number of authors to generalize Coulomb's law. With this in mind, we express the bottom shear stress in the following way

$$\tau_b = \rho g h \sin\theta = \tan\theta \rho g h \cos\theta = \sigma_b \tan\theta,$$

where $\sigma_b = \rho g h \cos\theta$ is the bottom normal stress. Then, assuming that the mean streamwise velocity depends on h and θ in the form

$$\bar{u} = A h^n \tan^m\theta, \tag{16}$$

it leads to a bulk flow curve in the form

$$\tau_b \propto \left(\frac{\bar{u}}{h^n}\right)^{1/m} \sigma_b. \tag{17}$$

We applied this variant to Pouliquen's data. From his data, we found $A = 10034$ s^{-1} m$^{-3.74}$, $n = 1.42$, and $m = 4.74$. Again, for the sake of simplicity, we posed $n = 3/2$ and $m = 5$ (giving $A = 17588$ s^{-1} m^{-4}). Figure 5 reports the variation of $K(I)\sigma_b$ as a function of τ_b, where $I = \bar{u}h^{-3/2}$ and $K(I) = I^{1/5}$, in a log-linear plot. As expected, Pouliquen's data collapse onto a single curve. As previously, the data scattering is very low. If we had to select the best scaling on the sole basis of a good agreement with a mean trend, there would be no specific reason to give preference to this scaling over the other found in § 3.2. In Fig. 5, the data obtained with the wider channel (glass beads $d = 1$ and 2 mm, $W = 48$ mm) form a well-defined curve, which matches Pouliquen's data, but there is a departure from the linear trend fit on those data. The data taken with the narrow channel reveal a similar trend, but are parallel to

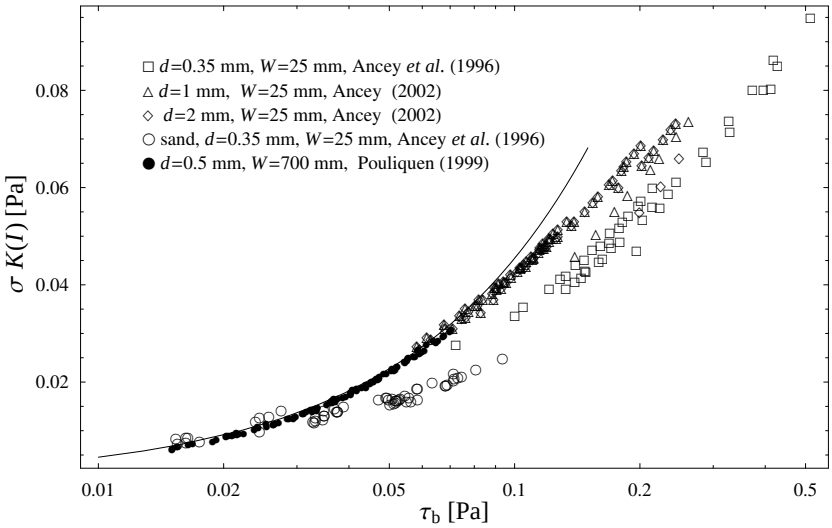

Fig. 5. Log-linear variation in $K(I)\sigma_b$ with $\tau_b = \rho g h \sin\theta$ for the data obtained by Pouliquen [31] (•), Ancey et al. [32] (□, ◯), and Ancey [33] (△, ◇); $K(I) = I^{1/5}$ is the bulk friction coefficient (to within a multiplicative constant) and $I = \bar{u}/h^{3/2}$ can be interpreted as the square root of the Savage number (to within a multiplicative constant). The solid line represents the linear trend $\tau_b = 2.08 K(I)\sigma_b$.

other data. This departure is expected because of the transition from regime A to regime B (which occurred when increasing the flow rate, i.e., the bottom shear stress).

More interesting is the structure of the scaling $\tau_b \propto K(I)\sigma_b$. The parameter K is dependent on the ratio $I = \bar{u}/h^{3/2}$. A dimensionless variant of this ratio is $I_2 = \rho(d\dot{\gamma})^2/\sigma_b \propto I^2$ (with d the particle diameter). It has been called the Savage number and interpreted in terms of the ratio of the collisional stress to the normal stress [39]. The dimensionless number I_2 comes up also in the form of a characteristic-time ratio in the derivation of the bulk stress tensor for the frictional-collisional regime, proposed by Ancey and Evesque [28]. In this theoretical model, the shear stress τ should vary as $F(I_2)\sigma$. Numerous numerical simulations carried out over the last 5 years have also shown that in a frictional-collisional regime, the stress ratio τ/σ is a function of the so-called inertial number $I_1 = d\dot{\gamma}/\sqrt{\sigma_b/\rho} \propto I$ [40]. From this physical point of view, the scaling $\tau_b \propto K(I)\sigma_b$ makes more sense than the one derived in Sect. 3.2. The only troublesome point is the shear stress τ dropping to zero when $I \to 0$, whereas one expects τ to tend toward a finite value, but recall that the same issue arose when investigating the Herschel-Bulkley case (see § 2.3).

It is also interesting to compare the friction law (14) derived by Pouliquen [31] with Eq. (17). Figure 6 shows the variation in the bulk friction coefficient $\hat{K}$ (dashed line); the dots represent the pairs of values ($\bar{u}$, h) used effectively by Pouliquen [31] to adjust Eq. (14). On the same log-linear plot, we report the

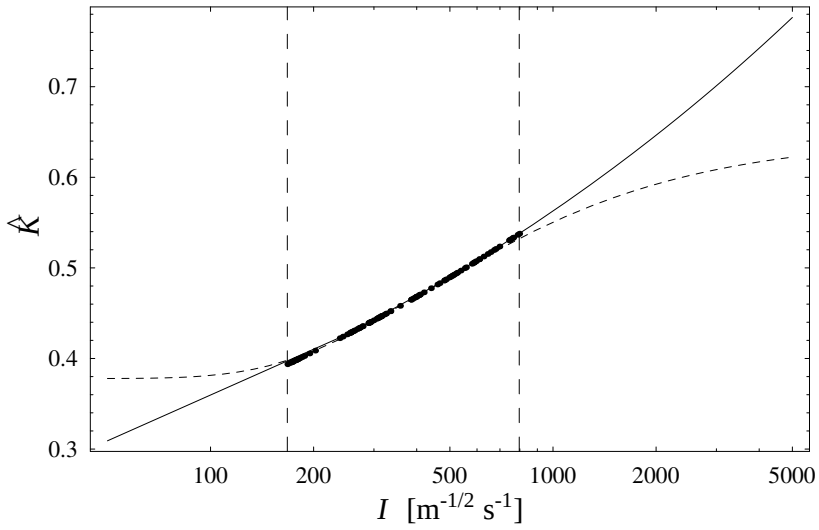

Fig. 6. Comparison of the friction coefficient $\hat{K}(I)$ computed using Eq. (17) (solid line) and Eq. (14) (Pouliquen's law, dashed line).

bulk friction coefficient

$$\hat{K} = 2.08K(I) = 2.08I^{1/5}, \tag{18}$$

fit on his data (solid line). As seen in this figure, over the domain where the measurements were taken, the two expressions coincide, but differ significantly outside of this domain. As usual when interpolating data, different curves can be used to interpolate the data with the same level of confidence, but proper extrapolation outside of the interpolation domain is trickier to ensure. We can think of other interpolating curves passing through the data. For instance, da Cruz et al. [40] proposed a straight line $\hat{K} = a + bI$, to represent the behavior in the frictional-collisional regime. Jop et al. [41] used a rational function for the same purpose. A different relation between the normal and shear stresses can be imagined, e.g., a relation in the form: $\tau = \hat{K}(I)\sigma + \hat{L}(I)$, with $\hat{K}$ and $\hat{L}$ power-law functions of I, and once again, it would be possible to fit the law on the data.

Instead of using Pouliquen's data to adjust the parameters n and m in the velocity equation (16), we can use the data obtained with 1-mm glass beads in [33]. In that case, we found: $n = 0.07$ and $m = 5.30$. For simplicity, we posed $n = 0$ and $m = 5$ (giving $A = 14.35$ s^{-1} m^{-4}), which led to a shear stress in the form

$$\tau_b \propto \bar{u}^{1/5}\sigma_b. \tag{19}$$

We define $M = \bar{u}^{1/5}$. Figure 7 shows the variation between τ_b and $M\sigma_b$ in a

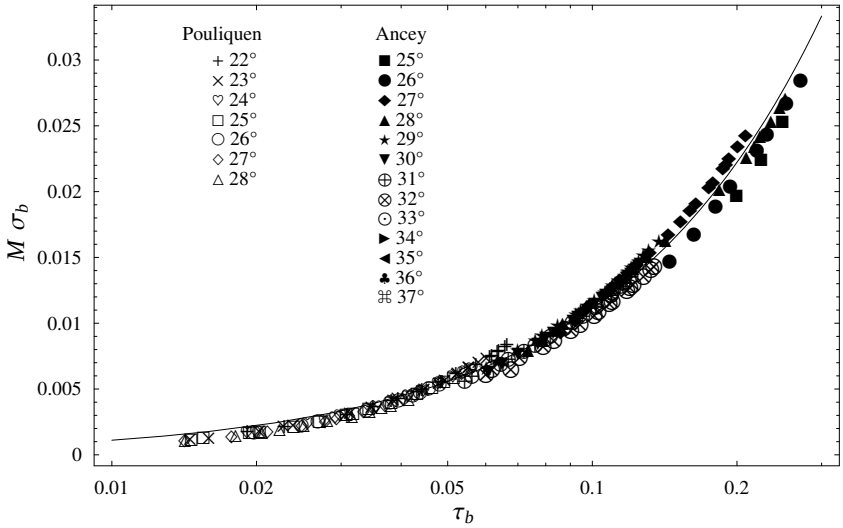

Fig. 7. Log-linear variation in $M\sigma_b$ with $\tau_b = \rho g h \sin\theta$. Pouliquen's data [31] together with Ancey's data (1-mm glass beads, channel width $W = 48$ mm [33]) are reported. The solid line represents the mean trend $\tau_b = \hat{M}\sigma_b$, with $\hat{M} = 9\bar{u}^{1/5}$.

log-linear plot. We have also plotted the mean trend

$$\tau_b = \hat{M}\sigma_b, \text{ with } \hat{M} = 9M = 9\bar{u}^{1/5}. \tag{20}$$

As seen in the figure, almost all the data collapse onto the mean trend independently of the flow regime (A or B), but a small departure is observed for the shallowest slopes for both Pouliquen's and Ancey's data (regime A). Contrary to $\hat{K}(I)$, which can be interpreted from the rheophysical point view as a competition between frictions and collisional contacts, there is no obvious interpretation for $\hat{M}$. From a purely continuum-mechanics point of view, the dependence on mean velocity is suspect since a constitutive parameter should be frame-independent and thus cannot depend on velocity alone; as for the Manning-Strickler relation used in open-channel hydraulics, this probably means that the true rheological behavior is much more complicated and depends on additional hidden variables (e.g., granular temperature, solid concentration).

From this discussion, it should be remembered that various expressions can be used to describe the behavior in the frictional-collisional regime. To date, no law fully describes all the data available for all regimes, but a few expressions provide reasonable estimates of the rheological behavior in a steady uniform regime for particular regimes. Their structure can be interpreted using dimensional analysis and rheophysical arguments. The main question lies in delimiting the frictional-collisional regime and defining the interpolation domain for these empirical curves. In the next section, we will see that the data obtained under time-dependent flow conditions offer a basis to further

test the bulk constitutive equations.

4 Leading edge

The shallow-flow equations (3–6) can be further used to test the rheological interpretation. Indeed, the flow-depth profile of the nose and the front velocity provide crucial information to check the consistency of a rheological interpretation or fit rheological parameters. For instance, the depth profile of a viscoplastic deposit can be used to estimate the yield stress [42, 43]. Here, we will provide another example of application by addressing Pouliquen's observations and their consequence in terms of rheological behavior.

A striking observation made by Pouliquen is that granular surges involving spherical glass beads down mild slopes propagated at constant velocity, whereas for most fluids, gravity induces an acceleration of the leading edge. Another remarkable feature revealed by Pouliquen is the self-similarity of the flow-depth profile: he observed that the shape of the head remained constant and independent of the body flow depth. Physically, this means that the head is a traveling wave and the flow-depth profile could be cast in the form

$$h(x,\ t) = h_b H(x - ct),$$

with c the front velocity and h_b the body thickness; H is a function enjoying the following properties: (i) $H(0) = 0$, at the front ($x = ct$) the flow depth drops to zero, (ii) $H(-\infty) = 1$, the flow depth at the rear of the head should match the flow depth of the body. In this section, we will take a closer look at this notable behavior to test the bulk constitutive equations worked out in § 3.

First note that Pouliquen [44] reported low curvatures of the free surface in the immediate vicinity of the front, which means that the shallow-flow approximation still holds within the tip region since the flow depth-to-length ratio remains small: $\epsilon = O(0.1)$. Then, to derive the flow-depth profile for the leading edge, Pouliquen [44] used the bulk momentum equation (6), and by assuming that the velocity was constant within the head, he obtained a differential equation

$$k\frac{dh}{dx} = \tan\theta - \mu,$$

which provided flow depths in full agreement with his experimental measurements. However, the assumption of a constant velocity within the nose (i.e., in a region where the free surface exhibited a significant curvature) is at first glance not consistent with his bulk constitutive equation. Indeed, this would

mean that either the nose acts as a rigid body (i.e., no deformation within the bulk and slipping along the bottom surface) or the flow-depth averaged velocity is independent of the flow depth, but both explanations conflict with observations.

- The former interpretation contrasts with experimental observations since many authors observed that granular flows down rough surfaces are sheared in the cross-stream direction.
- For the latter case, if the mean velocity keeps the same value at any point, there is an apparent paradox with Pouliquen's conclusion: indeed, we should have $\bar{u} \propto h^{3/2}$ (for the body) and at the same time $\bar{u}$ independent of h (within the tip region).

In fact, the mean velocity being independent of h means that the velocity profile in the cross-stream direction should be self-similar, i.e., in the form

$$u(y) = U(y/h),$$

the integration of which provides $\bar{u} = \int_0^1 U(\eta)d\eta$, which is independent of the flow depth as sought, while integrating twice gives a flow rate

$$q = h\bar{u} = h\int_0^1 U(\eta)d\eta \propto h,$$

which is a linear function of the flow depth. Interestingly enough, this result is reminiscent of the hallmark of regime B (see § 3.1) and if so, it would mean that the tip region is in regime B. Let us take a closer look at this issue.

Let us consider the x-momentum balance equation (6), with $\beta = 1$ for the sake of simplicity, for the leading edge. Since the head is assumed to be in regime B, the flow-depth averaged velocity is independent of the flow depth so that the advection term vanishes. We find

$$\tau_b = \rho g h \sin\theta \left(1 - k\cot\theta \frac{\partial h}{\partial x}\right).$$

This equation means that within the leading edge, the curvature of the free surface induces an increase in the bottom shear stress value by a factor $1 - k\cot\theta h_x > 1$ relative to its value achieved in the uniform regime (body). This also means that if we wish to use the same formulation as earlier for the uniform regime, we must take this correcting factor into account. For this purpose, we consider that the quantity $\sin\theta(1 - k\cot\theta h_x)$ is equivalent to an effective angle $\sin\theta'$. For instance, with $\theta = 25°$, $k = 1$, and $h_x \sim 0.1$, we find that the correcting factor is 1.21, which corresponds to an effective angle $\theta' = 30.9°$, which is larger than the internal friction angle ($\varphi \sim 28°$). In other

words, if for a given inflow rate and slope, the flow body is in regime A, the leading edge is likely to experience regime B (in Ancey's flume experiments, it was observed that increasing slope while retaining the flow rate leads to a transition to regime B). We could then imagine that the friction law depends on the bed angle in the following way:

$$\begin{cases} \theta < \varphi, \text{ then } \tau_b = \hat{K}(I)\sigma_b, \\ \theta > \varphi, \text{ then } \tau_b = \hat{M}(\bar{u})\sigma_b, \end{cases}$$

with $\hat{M}$ given by Eq. (20) while $\hat{K}$ is yielded by Eq. (14) ($\hat{K} = \mu$) or Eq. (18). With this law, we can retrieve the body behavior ($\bar{u} \propto h^{3/2}$) and explain why the head behaves like a traveling wave and the front velocity is constant and fixed by the flow depth of the body. The partitioning is, however, unsatisfactory since from the continuum point of view, a bulk constitutive equation cannot depend on the channel slope. This probably means that a more convenient expression is still to be worked out; in particular, a thorough investigation into the transition between regime A and regime B could provide a more sensible relation. The appendix presents more technical arguments, based on the method of characteristics, which also pleads in favor of the occurrence of regime B within the head.

Another possibility is directly in line with the active/passive pressure coefficient used in the Savage-Hutter theory [11]. In this theory, the coefficient k depends on the compression state of the material; if there is a positive velocity gradient in the streamwise direction ($\partial\bar{u}/\partial x > 0$, implying a stretching motion in the x-direction), k takes one value, whereas if the gradient is negative (material compaction), it takes another value [11]. We could imagine that a similar mechanism operates here and adjusts the shear stress when there is a pressure gradient; this also means that the behavior switch would be controlled by $\partial h/\partial x$ rather than $\partial\bar{u}/\partial x$ since convective acceleration is zero in Pouliquen's experiments.

Note also that Pouliquen systematically observed a layer deposited along the plane after the flow stopped. This may mean that the mass balance equation (3) is no longer satisfied because of deposition. A negative mass balance can be equivalent to a frictional force and if this scenario were valid, this could explain why the front moves at constant velocity, at least from a qualitative point of view.

All these explanations are speculative for now and further work is needed to elucidate this point.

5 Concluding remarks

The objective of this paper was to develop a method for deriving the bulk constitutive relation $\tau_b = F(\bar{u}, h)$, which is quite general and objective, i.e., it can be applied to any type of fluid with a minimum of additional assumptions. The method can be seen as an attempt to generalize Manning-Strickler-like relations to non-Newtonian flows, i.e., we use the shallow-flow equations to compute the flow features and assume that flow resistance can be expressed as a monomial power function of $\bar{u}$ and h.

A more accurate method was already proposed in a paper by Ancey et al. [32], but it relied on the crucial assumption that there is a one-to-one relation between the shear stress and the shear rate $\tau = F(\dot{\gamma})$, which in turn implies that the bulk constitutive relation must be in the form $\tau_b = F(\bar{u}/h)$. In this paper, we relax this condition and seek relations of the form $\tau_b = F(\bar{u}, h)$, where the bottom shear stress can be expressed as a monomial function of $\bar{u}$ and h, i.e., $F(\bar{u}, h) \propto u^p h^n$. This means that we cannot obtain the constitutive equation $\tau = F(\dot{\gamma}, \sigma)$, but only a bulk estimate $\tau_b = F(\bar{u}, h)$ (i.e., the bottom shear stress).

Applications to simple fluids revealed the potential of this simple method. More interesting was the application to complex fluids. Dry granular flows offer a perfect field of investigation because of the wealth of properties exhibited. We first applied the method to the experimental data obtained by Pouliquen [31]. We found that $\tau_b \propto \bar{u}^{1/6} h^{3/4}$ properly represents the bottom shear stress measured experimentally. Application to other sets of data also showed that this scaling may be a good candidate for representing bulk rheological behavior. The point was that there is no easy physical interpretation for this scaling. It is, however, possible to amend it by providing additional information on the form of the constitutive equation (see § 3.3). We thus sought a generalized Coulomb's law, where the bottom shear stress is linearly linked to the bottom normal stress σ_b: $\tau_b = \hat{K}\sigma_b$. From Pouliquen's data, we found that $\hat{K} = 2.08 I^{1/5}$, with $I = \bar{u}/h^{3/2}$, offered a correct representation of the rheological behavior. Applying the method to the data (which covered a wider range of flow regimes) obtained by Ancey [33] provides another scaling for the generalized Coulomb law: $\tau_b = \hat{M}\sigma_b$, with $\hat{M} = 9\bar{u}^{1/5}$, which provides a reasonably good description of the bottom shear variation for dry granular flows in both regimes A and B. The reason why the two relations do not differ much stems from the power of h. In the bulk friction coefficient $\hat{K} = 2.08 I^{1/5}$, the flow depth h rises to the power $-3/10$, which means that if we remove h from this expression, few significant changes are expected, since we are working with quite narrow ranges of flow depths (typically less than one order of magnitude). An indispensable condition to gain insight into the true rheological behavior would be to explore a wider range of flow depths, i.e., 2 or 3 orders

of magnitude, but we are likely to face regime transitions (as here, between regimes A and B).

To test the reliability of the bulk constitutive equations and discriminate them, we used additional observations of the time-dependent behavior of avalanching flows. A remarkable feature of granular surges revealed by Pouliquen's investigation is that the head behaves like a traveling wave and propagates at a constant velocity, in contrast with most fluids placed in a similar flow geometry. To put together the different pieces of the puzzle, we suggested a dependence of the bulk constitutive relation on the flow regime:

- the body is in regime A, i.e., $\bar{u} \propto h^{3/2}$ and τ_b is given by Pouliquen's relation (14) or alternative representations such as Eq. (18). The friction coefficient depends on the Savage number I_2 (or equivalently the inertia number I_1);
- the head is in regime B, i.e., the mean velocity is constant everywhere, independent of h, and fixed by the body's velocity. In that case, $\tau_b = \hat{M}\sigma_b = 9\bar{u}^{1/5}\sigma_b$, i.e., we have a Coulomb-like behavior, whose bulk friction angle is velocity-dependent.

We stress that this partitioning into two frictional laws is not very satisfactory and calls for further work to elucidate a number of unclear points discussed in § 4.

The method proposed in this paper is quite simple and has the potential to provide useful information on the rheological behavior from field or laboratory measurements. The minimum requirement is to have a sufficient number of data on mean velocity and flow depth for a sufficiently wide range of bed inclinations. Since it is systematic and relies on well-posed assumptions, this method is also useful in exploring the various forms that a bulk constitutive equation can take to describe steady uniform flows.

The application to real data also reveals the limits of this method since several bulk constitutive equations, which are structurally different, can be adjusted on the data. This would cause no trouble as long as one works within the interpolation domain of these equations, but can be quite dangerous whenever one tries to extrapolate these relations beyond their validity domain. Unfortunately, this may be the case when applying constitutive relations established on the laboratory scale to full-scale geophysical flows. For natural materials, there is a serious scaling issue that may undermine the value of laboratory experiments when used to interpret full-scale natural events [45]. For instance, is there any relation between the friction coefficient measured with a shear cell and the bulk friction coefficient of a snow avalanche? Essentially, all these empirical models hold true for a limited range of flow conditions and geometries. Part of the difficulty lies in the substantial changes in the flow properties in response to minute changes in the flow conditions. For instance for dry gran-

ular flows, bottom roughness plays a key role, which has been elucidated to a large degree for rapid collisional flows, but remains poorly understood for the frictional-collisional regime [46]. When a finite volume of dry granular material is released down a relatively smooth flume, the mass accelerates, then decelerates without reaching equilibrium [4, 47]. In contrast, equilibrium is reached when the bottom is rough or made up of an erodible bed [48].

Appendix

A remarkable feature of granular surges discovered by Pouliquen [31] is the front advancing at constant velocity, whereas for all fluids we are aware of, the front accelerates and ultimately becomes unstable. To better understand this issue, we use the method of characteristics to determine the position and velocity of the front. This method is very efficient not only for deriving analytical solutions, but also for understanding how information is conveyed. The basic idea is to transform the mass and momentum balance equations (3) and (6) into a pair of ordinary differential equations.

Multiplying the continuity equation (3) by $\eta = (kg\cos\theta h + (\beta-1)\bar{u}^2)/h/(\bar{u}(\beta-1)+f)$ with $f = \sqrt{kg\cos\theta h + \beta(\beta-1)\bar{u}^2}$ and adding the momentum balance equation (6), we transform the equations of motion into their characteristic form

$$\eta\frac{dh}{dt} + \frac{d\bar{u}}{dt} = g\sin\theta - \frac{\tau_b}{\rho h} \quad \text{on} \quad \frac{dx}{dt} = \lambda_+, \tag{.1}$$

where λ_+ is the forward characteristic velocity: $\lambda_+ = \beta\bar{u} + f$. The position of the front x_f can be determined by taking the limit $h \to 0$. However, the limit of $\eta dh/dt$ is not properly defined since $\eta \to \infty$ when $h \to 0$. To determine this limit, we are seeking the function (Riemann variable) ϕ such that $\mu d\phi = \eta dh + d\bar{u}$, where μ is an integrating factor. We failed to find an analytical solution, but an approximate solution can be obtained using a power-series expansion: $\phi = \phi_0 + (1-\beta)\phi_1 + (1-\beta)^2\phi_2 + \cdots$. We found $\mu = 1$, $\phi_0 = \bar{u} + 2\sqrt{gk\cos\theta h}$ and $\phi_1 = -4\bar{u} - \bar{u}^2(gk\cos\theta h)^{-1/2} - 3\phi_0\ln h$. If $\beta > 1$, we note that $\phi_1 \to \infty$ when $h \to 0$ and that the characteristic velocity $\lambda_+ = \beta\bar{u}$ is higher than the fluid velocity u; this means that, at least close to the leading edge, we must take $\beta = 1$ (i.e., the cross-stream velocity profile must be uniform) for the shallow-flow approach to be physically consistent. If $\beta = 1$, then $\phi = \lambda_+ = \bar{u}$ when $h \to 0$. The front position is then governed by

$$\frac{dx_f}{dt} = u_f \text{ and } \frac{du_f}{dt} = g\sin\theta - \lim_{h\to 0}\frac{F(\bar{u},\ h)}{\rho h}, \tag{.2}$$

with $\tau_b = F(\bar{u}, h)$. The only possibility of observing a front propagating with a constant velocity is that $\lim_{h\to 0} F/(\rho h) = g\sin\theta$, i.e., the bottom shear stress

exactly counterbalances the gravity acceleration for any slope. Note that most bulk constitutive relations fail to meet this condition, whereas the relation $F(\bar{u}, h) = \hat{M}\sigma_b = \rho g h \bar{u}^{1/5} \cos\theta$ satisfies it, which substantiates the analysis presented in Sect. 4.

A troublesome aspect in the use of the flow-depth averaged equations is the Boussinesq coefficient β tending toward unity, whereas there is clear evidence that for this type of free-surface flow, the entire flow depth is sheared within the body, implying that $\beta > 1$ far from the front. Interpreting the governing equations (3) and (6) in light of Pouliquen's experiments, we would expect there to be a significant alteration in the velocity profile within the head, with a self-similar profile tending to be uniform when one approaches the front. Such a significant change remains difficult to imagine from a purely two-dimensional kinematic point of view, but we can get around this problem if we assume that the head has a three-dimensional structure grains recirculating from the center-line to the side. This scenario is plausible given the shape of the head for this type of flow [49]: in contrast with Pouliquen's observations, some experiments and numerical simulation show that the contact line is not a straight line, but rather a parabolic line, whatever the flume width. If so, this also means that to properly analyze the head behavior, we should use two-dimensional governing equations rather a one-dimensional model. Another explanation of the odd behavior of β lies in a shortcoming of the shallow-flow equations when computing the head structure; indeed, a similar problem arises with the front non-Boussinesq gravity currents [50].

Acknowledgements

The work presented here was supported by the Swiss National Science Foundation under grant number 200021-105193, the competence center in Mobile Information and Communication Systems (a center supported by the Swiss National Science Foundation under grant number 5005-67322, MICS project), the competence center in Environmental Sciences (TRAMM project), and specific funds provided by EPFL (*vice-présidence à la recherche*).

References

[1] B. Saint Venant, Théorie du mouvement non permanent des eaux, avec application aux crues des rivières et à l'introduction des marées dans leur lit, C. R. Acad. Sci. Paris sér. I 173 (1871) 147–154– 237–240.

[2] E. Eglit, Some mathematical models of snow avalanches, in: M. Shahin-

poor (Ed.), Advances in the Mechanics and the Flow of Granular Materials, Trans Tech Publications, Clausthal-Zellerfeld, 1983, pp. 577–588.
[3] C. Ancey, Snow avalanches, in: N. Balmforth, A. Provenzale (Eds.), Geomorphological Fluid Mechanics: Selected Topics in Geological and Geomorphological Fluid Mechanics, Springer, Berlin, 2001, pp. 319–338.
[4] S.P. Pudasaini, K. Hutter, Avalanche Dynamics, Springer, Berlin, 2006.
[5] R.M. Iverson, The physics of debris flows, Rev. Geophys. 35 (1997) 245–296.
[6] R.M. Iverson, R.P. Denlinger, Flow of variably fluidized granular masses across three-dimensional terrain. 1. Coulomb mixture theory, J. Geophys. Res. 106 (2001) 537–552.
[7] C.C. Mei, K.F. Liu, M. Yuhi, Mud flows – Slow and fast, in: N. Balmforth, A. Provenzale (Eds.), Geomorphological Fluid Mechanics: selected topics in geological and geomorphological fluid mechanics, Springer, Berlin, 2001, pp. 548–577.
[8] P. Coussot, Mudflow Rheology and Dynamics, Balkema, Rotterdam, 1997.
[9] R.W. Griffiths, The dynamics of lava flows, Annu. Rev. Fluid Mech. 32 (2000) 477–518.
[10] N.J. Balmforth, A.S. Burbridge, R.V. Craster, Viscoplastic models of isothermal lava domes, J. Fluid Mech. 403 (2000) 37–65.
[11] S.B. Savage, K. Hutter, The motion of a finite mass of granular material down a rough incline, J. Fluid Mech. 199 (1989) 177–215.
[12] S.B. Savage, Flow of granular materials, in: P. Germain, J.-M. Piau, D. Caillerie (Eds.), Theoretical and Applied Mechanics, Elsevier, Amsterdam, 1989, pp. 241–266.
[13] R.M. Iverson, J. Vallance, New views of granular mass flows, Geology 29 (2002) 115–118.
[14] C. Ancey, Plasticity and geophysical flows: A review, J. Non-Newtonian Fluid Mech. 142 (2007) 4–35.
[15] F. Darve (Ed.), Geomaterials: Constitutive Equations and Modeling, Elsevier, London, 1989.
[16] J.T. Jenkins, Balance laws and constitutive relations for rapid flows of granular materials, in: J. Chandra, R. Srivastav (Eds.), Constitutive Models of Deformation, SIAM, Philadelphia, 1987, pp. 109–119.
[17] I. Goldhirsch, Rapid granular flows, Annu. Rev. Fluid Mech. 35 (2003) 267–293.
[18] S.B. Savage, Granular flows down rough inclined - Review and extension, in: J. Jenkins, M. Satake (Eds.), U.S./ Japan Seminar on New Models and Constitutive Relations in the Mechanics of Granular Materials, Elseviers Science Publishers, Amsterdam, Ithaca, 1982, pp. 261–282.
[19] P.C. Johnson, R. Jackson, Frictional-collisional equations of motion particulate flows and their application to chutes, J. Fluid Mech. 210 (1990) 501–535.
[20] A. Berker, W. Van Arsdale, Phenomenological models of viscoplastic,

thixotropic, and granular materials, Rheol. Acta 31 (1992) 119–138.
[21] M. Louge, Model for dense granular flows down bumpy inclines, Phys. Rev. E 061303 (2003) 061303.
[22] C. Josserand, P.-Y. Lagrée, D. Lhuillier, Stationary shear flows of dense granular materials: a tentative continuum modelling, Eur. Phys. J. E 14 (2004) 127–135.
[23] S.B. Savage, Free-surface granular flows down heaps, J. Eng. Math. 60 (2007) 221–240.
[24] D. Ertas, G.S. Grest, T.C. Hasley, D. Levine, L.E. Silbert, Gravity-driven dense granular flows, Europhys. Lett. 56 (2001) 214–220.
[25] E. Aharonov, D. Sparks, Shear profiles and localization in simulations of granular materials, Phys. Rev. E 65 (2002) 051302.
[26] L. Staron, E.J. Hinch, Study of the collapse of granular columns using two-dimensional discrete-grain simulation, J. Fluid Mech. 545 (2005) 1–27.
[27] P. Mills, D. Loggia, M. Tixier, Model for a stationary dense granular flow along an inclined wall, Europhysis Letters 45 (1999) 733–738.
[28] C. Ancey, P. Evesque, Frictional-collisional regime for granular suspension flows down an inclined channel, Phys. Rev. E 62 (2000) 8349–8360.
[29] GDR-MIDI, On dense granular flows, Eur. Phys. J. E 14 (2004) 341–365.
[30] P. Jop, O. Pouliquen, Y. Forterre, A constitutive law for dense granular flows, Nature 441 (2006) 727–730.
[31] O. Pouliquen, On the shape of granular front down rough inclined planes, Phys. Fluids 11 (1999) 1956–1958.
[32] C. Ancey, P. Coussot, P. Evesque, Examination of the possibility of a fluid-mechanics treatment for dense granular flows, Mech. Cohesive-Frict. Mater. 1 (1996) 385–403.
[33] C. Ancey, Dry granular flow down an inclined channel: Experimental investigations on the frictional-collisional regime, Phys. Rev. E 65 (2002) 011304.
[34] F. Bouchut, A. Mangeney-Castelnau, B. Perthame, J.-P. Vilotte, A new model of Saint Venant and Savage-Hutter type for gravity driven shallow flows, C. R. Acad. Sci. Paris sér. I 336 (2003) 531–536.
[35] J.B. Keller, Shallow-water theory for arbitrary slopes of the bottom, J. Fluid Mech. 489 (2003) 345–348.
[36] B.D. Coleman, H. Markowitz, W. Noll, Viscometric flows of non-Newtonian fluids, Vol. 5 of Springer Tracts in natural philosophy, Springer-Verlag, Berlin, 1966.
[37] G. Barenblatt, Scaling, Self-Similarity, and Intermediate Asymptotics, Cambridge University Press, Cambridge, 1996.
[38] G. Keulegan, Laws of turbulent flows in open channels, J. Res. Natl Bur. Stand. 21 (1938) 707–741.
[39] S.B. Savage, The mechanics of rapid granular flows, Adv. Appl. Mech. 24 (1984) 289–366.
[40] F. da Cruz, S. Emam, M. Prochnow, J.-M. Roux, F. Chevoir, Rheo-

physics of dense granular materials: Discrete simulation of plane shear flows, Phys. Rev. E 72 (2005) 021309.
[41] P. Jop, Y. Forterre, O. Pouliquen, Crucial role of side walls for granular surface flows: consequences for the rheology, J. Fluid Mech. 541 (2005) 167–192.
[42] P. Coussot, S. Proust, C. Ancey, Rheological interpretation of deposits of yield stress fluids, J. Non-Newtonian Fluid Mech. 66 (1996) 55–70.
[43] D.I. Osmond, R.W. Griffiths, The static shape of yield strength fluids slowly emplaced on slopes, J. Geophys. Res. B 106 (2001) 16241–16250.
[44] O. Pouliquen, Scaling laws in granular flows down rough inclined planes, Phys. Fluids 11 (1999) 542–548.
[45] R.M. Iverson, How should mathematical models of geomorphic processus to be judged?, in: P. Wilcock, R. Iverson (Eds.), Prediction in Geomorphology, American Geophysical Union, Washington, D.C., 2003, pp. 83–94.
[46] L.E. Silbert, G.S. Grest, S.J. Plimpton, D. Levine, Boundary effects and self-organization in dense granular flows, Phys. Fluids 14 (2002) 2637–2646.
[47] T. Koch, R. Greve, K. Hutter, Unconfined flow of granular avalanches along a partly curved surface. II. Experiments and numerical computations, Proc. R. Soc. London ser. A 445 (1994) 415–435.
[48] A. Daerr, Dynamical equilibrium of avalanches on a rough plane, Phys. Fluids 13 (2001) 2115–2124.
[49] G. Félix, N. Thomas, Relation between dry granular flow regimes and morphology of deposits: formation of levées in pyroclastic deposits, Earth Planet. Sci. Lett. 221 (2004) 197–213.
[50] C. Ancey, S. Cochard, S. Wiederseiner, M. Rentschler, Existence and features of similarity solutions for supercritical non-Boussinesq gravity currents, Physica D 226 (2007) 32–54.